JBC RESEARCH ARTICLE

HIV-1 exposure promotes PKG1-mediated phosphorylation and degradation of stathmin to increase epithelial barrier permeability

Received for publication, October 5, 2020, and in revised form, March 29, 2021 Published, Papers in Press, April 9, 2021,
https://doi.org/10.1016/j.jbc.2021.100644

Wei Xie[1], Mingzhen Chen[1], Zhaodong Zhai[1], Hongjie Li[1], Ting Song[1], Yigao Zhu[1], Dan Dong[1], Peng Zhou[1], Liangwei Duan[2], You Zhang[2], Dengwen Li[2], Xinqi Liu[2], Jun Zhou[1,2,*], and Min Liu[1,*]

From the [1]Shandong Provincial Key Laboratory of Animal Resistance Biology, Collaborative Innovation Center of Cell Biology in Universities of Shandong, Institute of Biomedical Sciences, College of Life Sciences, Shandong Normal University, Jinan, Shandong, China; [2]State Key Laboratory of Medicinal Chemical Biology, College of Life Sciences, Nankai University, Tianjin, China

Edited by Alex Toker

Exposure of mucosal epithelial cells to the human immunodeficiency virus type 1 (HIV-1) envelope glycoprotein gp120 is known to disrupt epithelial cell junctions by impairing stathmin-mediated microtubule depolymerization. However, the pathological significance of this process and its underlying molecular mechanism remain unclear. Here we show that treatment of epithelial cells with pseudotyped HIV-1 viral particles or recombinant gp120 protein results in the activation of protein kinase G 1 (PKG1). Examination of epithelial cells by immunofluorescence microscopy reveals that PKG1 activation mediates the epithelial barrier damage upon HIV-1 exposure. Immunoprecipitation experiments show that PKG1 interacts with stathmin and phosphorylates stathmin at serine 63 in the presence of gp120. Immunoprecipitation and immunofluorescence microscopy further demonstrate that PKG1-mediated phosphorylation of stathmin promotes its autophagic degradation by enhancing the interaction between stathmin and the autophagy adaptor protein p62. Collectively, these results suggest that HIV-1 exposure exploits the PKG1/stathmin axis to affect the microtubule cytoskeleton and thereby perturbs epithelial cell junctions. Our findings reveal a novel molecular mechanism by which exposure to HIV-1 increases epithelial permeability, which has implications for the development of effective strategies to prevent mucosal HIV-1 transmission.

Human immunodeficiency virus type 1 (HIV-1) affects millions of people worldwide. The major routes of HIV-1 transmission are percutaneous injury (blood or bodily fluid), cutaneous injury (skin wound), and contact with mucous membranes. In most cases (>90%), HIV-1 infection is initiated *via* different mucosal (*e.g.*, genital, rectal, and occasionally oral) epithelial surfaces after sexual contact (1, 2) and is associated with increased mucosal permeability (3). Various vaccines and topical microbicides have been developed that interfere with viral transmission based on current knowledge of the initial steps of mucosal penetration by HIV-1 (4, 5).

The HIV-1 envelope glycoprotein gp120 binds to its primary receptor cluster of differentiation 4 (CD4) and chemokine coreceptors, including C-C chemokine receptor type 5 (CCR5) and C-X-C chemokine receptor type 4 (CXCR4), and undergoes entry-related conformational changes (6). CCR5 and CXCR4 are expressed in genital, intestinal, and oral mucosal membranes. The attachment of HIV-1 viral particles to the mucosal membrane depends on the interaction of gp120 with its chemokine coreceptors. The mucosal epithelium functions as a selectively permeable barrier through the formation of cell junctions, including tight and adherens junctions, which are multiprotein complexes that connect adjacent epithelial cells (7, 8). HIV-1 gp120 has been shown to compromise the mucosal barrier by disruption of these junctions, resulting in increased epithelial permeability (2).

The microtubule cytoskeleton participates in a variety of cellular activities including cell motility, division, shaping, and intracellular trafficking (9). In addition, microtubules play an important role in the formation and maintenance of cell junctions (10–12). Microtubules bind to the adherens junction protein α-catenin *via* the centrosome-associated protein 350 (CAP350), which can influence the movement of adherens junction proteins within the cytoplasm and their distribution at the cell cortex (13). The minus ends of microtubules are linked to E-cadherin/p120 catenin by the calmodulin-regulated spectrin-associated protein 3 (CAMSAP3)/pleckstrin homology domain-containing A7 (PLEKHA7) complex, to maintain the integrity and stability of adherens junctions (14). Microtubules are also critical for the assembly of tight junctions by promoting CAMSAP3/PLEKHA7-dependent recruitment of paracingulin and zona occludens 1 (ZO-1) (15, 16).

We have previously demonstrated that interaction of gp120 with mucosal epithelial cells induces autophagic degradation of the microtubule-destabilizing protein stathmin. The consequent reduction in stathmin levels leads to microtubule hyperstabilization and disruption of junctional complexes, allowing HIV-1 to reach and attack human immune cells (17). However, the pathological relevance and molecular basis of these events are unknown. In this study, we report a previously

* For correspondence: Jun Zhou, junzhou@sdnu.edu.cn; Min Liu, minliu@sdnu.edu.cn.

undescribed mechanism by which exposure of mucosal epithelial cells to HIV-1 breaches the mucosal barrier to initiate the infection cycle. We show that HIV-1 exposure activates protein kinase G (PKG) 1 to phosphorylate stathmin at serine 63, thereby promoting its degradation *via* autophagy. This in turn triggers microtubule hyperstabilization and disassembly of the junctional complex, leading to the disruption of the mucosal barrier.

Results

HIV-1 pseudoviruses damage cell junctions by inducing stathmin degradation and microtubule hyperstabilization

To investigate the clinical significance and molecular basis of mucosal barrier disruption by HIV-1 gp120, we examined the integrity of cell junctions based on the localization of the tight junction marker, ZO-1, and the adherens junction marker, E-cadherin (18–20). Caco-2 human colon cancer cells were incubated with envelope (Env)-pseudotyped HIV-1 or vesicular stomatitis virus glycoprotein (VSVG)-pseudotyped control viruses. The junctional localization of ZO-1 and E-cadherin was decreased upon HIV-1 exposure (Fig. 1, *A–D*). AMD3100 is a CXCR4 antagonist that has been shown to specifically inhibit HIV-1 entry and membrane fusion by blocking interaction of the virus with CXCR4 (21). AMD3100 treatment abrogated the decrease in ZO-1 and E-cadherin junctional signals following HIV-1 exposure (Fig. 1, *A–D*).

Microtubules play an important role in the delivery of junctional proteins to cell contact sites and the assembly of junctional complexes (15, 17, 22). We performed immunofluorescence labeling to detect acetylated α-tubulin, a marker of stabilized microtubules (23), and found that incubation with HIV-1 pseudoviruses caused microtubule hyperstabilization in Caco-2 cells (Fig. 1, *E* and *F*). To examine the relationship between HIV-1 exposure and microtubule organization, we used AMD3100 to block HIV-1 interaction with CXCR4.

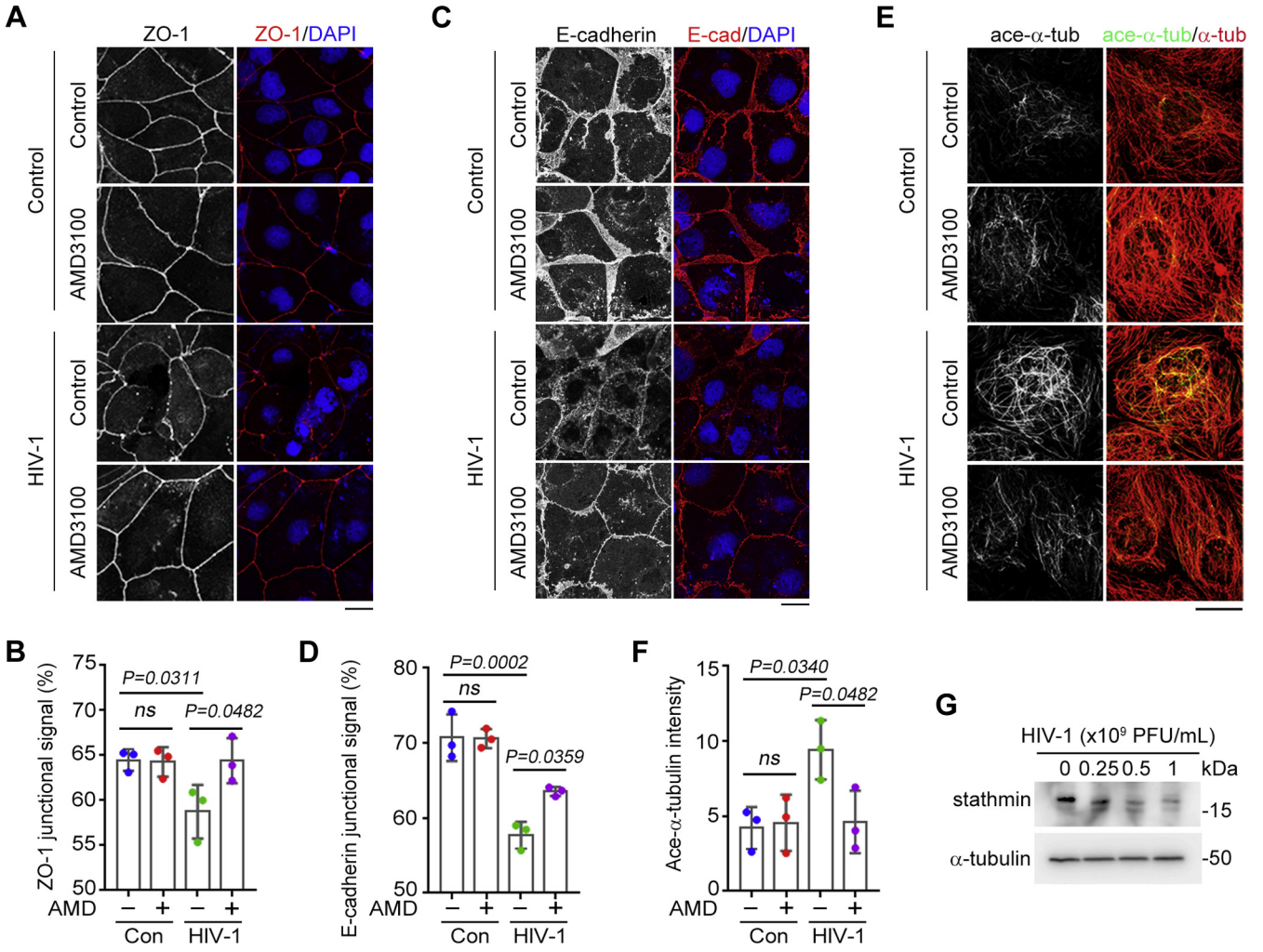

Figure 1. Exposure to Env-pseudotyped HIV-1 decreases the stathmin level and hyperstabilizes microtubules to disrupt cell junctions. *A* and *C*, immunofluorescence labeling of ZO-1 (*A*) and E-cadherin (*C*) in Caco-2 cells treated with Env-pseudotyped HIV-1 or VSVG-pseudotyped control viruses (1×10^9 PFU/mL) with or without AMD3100 (10 μM) for 24 h. Scale bars, 25 μm. *B* and *D*, graphs showing the mean ZO-1 (*B*) and E-cadherin (*D*) fluorescence at cell junctions. $n = 3$ biological replicates. *E*, immunofluorescence labeling of α-tubulin and acetylated α-tubulin in Caco-2 cells treated with HIV-1 or control viruses with or without AMD3100 for 24 h. Scale bar, 20 μm. *F*, graphs showing the fluorescence intensity of acetylated α-tubulin. $n = 3$ biological replicates. *G*, Caco-2 cells were treated with HIV-1 for 24 h, and cell lysates were collected and analyzed by immunoblotting. Data are presented as mean ± SD. ns, not significant.

Microtubule hyperstabilization was largely reversed by AMD3100 treatment (Fig. 1, *E* and *F*). Microtubule assembly from α/β-tubulin heterodimers is inhibited by microtubule-destabilizing proteins such as stathmin (24–26). We observed that exposure to HIV-1 pseudoviruses decreased the level of stathmin in Caco-2 cells (Fig. 1*G*), consistent with the finding that HIV-1 exposure hyperstabilizes microtubules. Thus, downregulation of stathmin leads to microtubule hyperstabilization, allowing HIV-1 to compromise epithelial cell junctions.

PKG1 interacts with stathmin and causes epithelial barrier damage upon exposure to HIV-1

To investigate the molecular link between HIV-1 exposure and stathmin degradation, we immunoprecipitated green fluorescent protein (GFP)-tagged stathmin from transfected HEK293T cells and examined stathmin-interacting proteins by mass spectrometry. Two candidate proteins were identified, namely, PKG1 and AarF domain-containing kinase 3 (ADCK3) (Fig. 2, *A* and *B*, and Table S1).

As phosphorylation is an important regulator of protein kinase activity, we examined the activity of PKG1 and ADCK3 following HIV-1 exposure. HIV-1 gp120 increased the serine/threonine phosphorylation of PKG1 (Fig. 2*C*), indicating its activation, whereas ADCK3 phosphorylation was unaffected (Fig. 2*D*). Moreover, small interfering RNA (siRNA)-mediated knockdown of PKG1 enhanced junctional ZO-1 and E-cadherin signals in the presence of HIV-1 gp120 (Fig. 2, *E*–*H*). On the other hand, ADCK3 knockdown did not abrogate the decrease in junctional ZO-1 and E-cadherin localization (Fig. 2, *E*–*H*). These results suggest that HIV-1 exposure results in the activation of PKG1, which might be

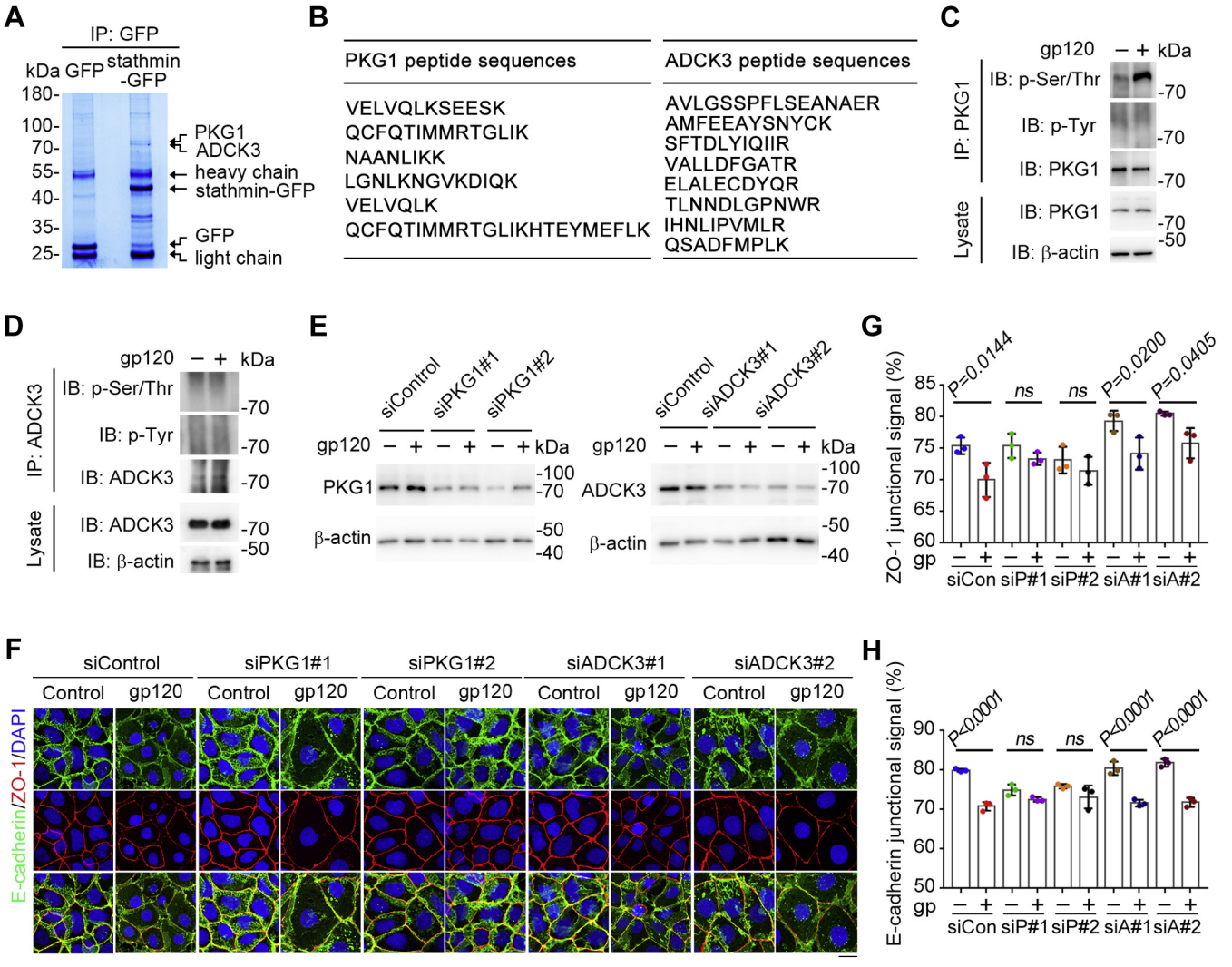

Figure 2. PKG1 is activated by HIV-1 gp120 and mediates its disruption of cell junctions. *A*, immunoprecipitation and coomassie blue staining showing the interaction of proteins with stathmin-GFP in HEK293T cells. *B*, PKG1 or ADCK3 peptide sequences identified by mass spectrometry in the proteins immunoprecipitated from stathmin-GFP expressed HEK293T lysates with the GFP-beads. *C*, immunoprecipitation and immunoblotting results showing the phosphorylation of endogenous PKG1 in RKO cells with 0 or 1 μg/mL gp120 treatment. *D*, immunoprecipitation and immunoblotting results showing the phosphorylation of endogenous ADCK3 in RKO cells with or without gp120 treatment. *E*, immunoblotting results showing the knockdown efficiency of PKG1 or ADCK3 in Caco-2 cells. *F*, immunolabeling of ZO-1 or E-cadherin in cells incubated with gp120 for 24 h after PKG1 or ADCK3 knockdown. Scale bar, 10 μm. *G* and *H*, analysis of ZO-1 (*G*) or E-cadherin (*H*) fluorescence intensity at cell junctions. $n = 3$ biological replicates. Data are presented as mean ± SD. ns, not significant.

related to stathmin degradation and microtubule reorganization.

PKG1 binds and phosphorylates stathmin in the presence of HIV-1 Gp120

PKG1 is a serine/threonine protein kinase that is activated by cyclic GMP and regulates diverse signal transduction pathways. We examined the molecular relevance of PKG1 in HIV-1-induced degradation of stathmin by immunoprecipitation and pulldown experiments. Reciprocal immunoprecipitation of PKG1-Flag and stathmin-GFP revealed an interaction between the two proteins in HEK293T cells (Fig. 3, *A* and *B*). The His pulldown assay confirmed their direct interaction *in vitro* (Fig. 3*C*). Furthermore, endogenous PKG1 coimmunoprecipitated with stathmin in intestinal, oral, and vaginal epithelial cells (Fig. 3*D*), indicating that PKG1 and stathmin interact *in vivo*.

Stathmin undergoes extensive phosphorylation in response to various extracellular factors, and its tubulin-sequestering capacity is weakened by phosphorylation at one or more of its four conserved serine residues (serine 16, 25, 38, and 63) (27, 28). Based on these findings, we investigated whether the interaction between PKG1 and stathmin leads to stathmin phosphorylation by coexpressing PKG1-Flag and stathmin-GFP in Ca9-22 cells. PKG1 overexpression increased stathmin serine/threonine phosphorylation (Fig. 3*E*), suggesting that stathmin is a substrate of PKG1; this was accompanied by a decrease in stathmin protein levels, implying that

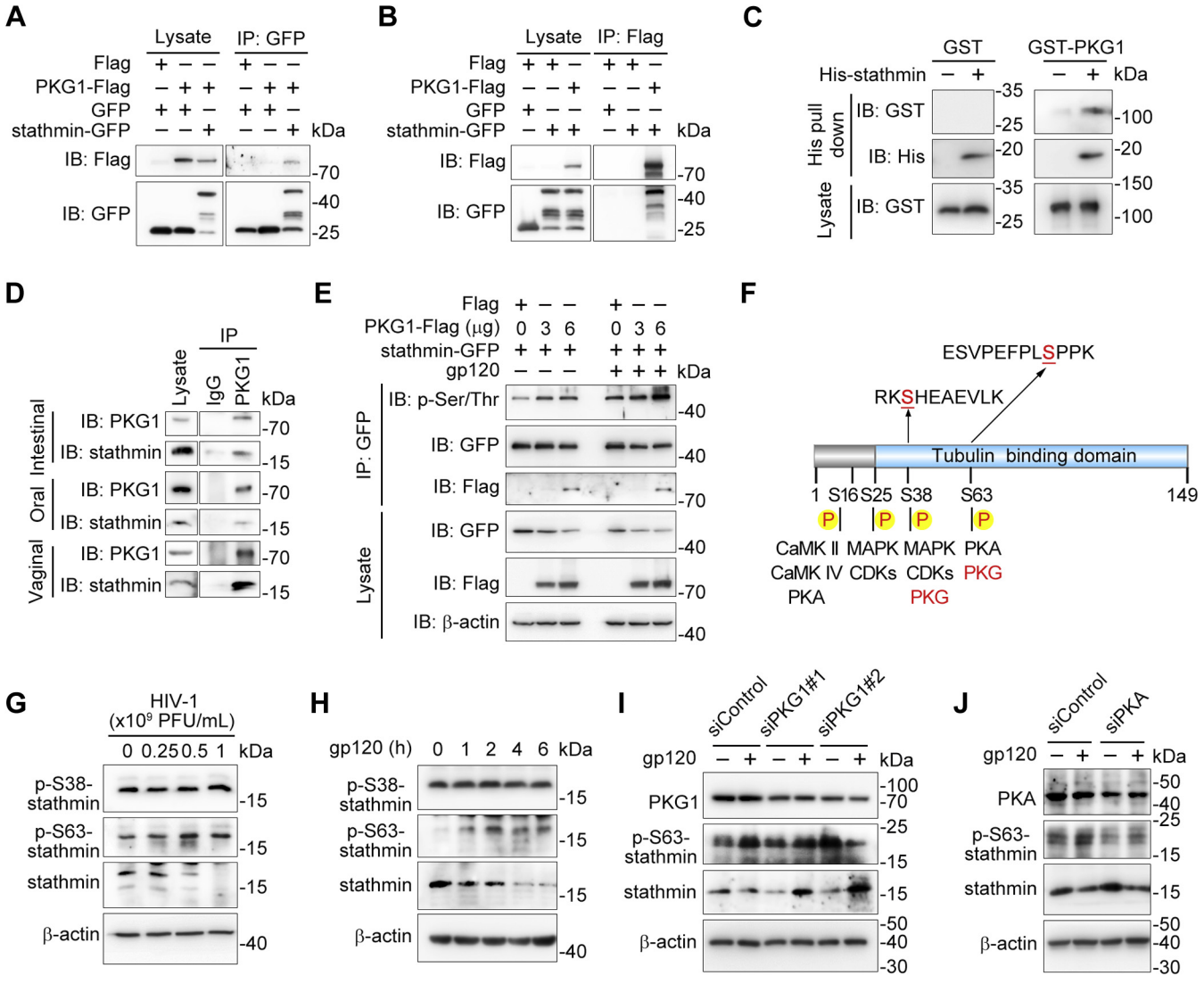

Figure 3. PKG1 interacts with stathmin and phosphorylates stathmin at serine 63. *A* and *B*, immunoprecipitation and immunoblotting results showing the interaction of PKG1-Flag and stathmin-GFP in HEK293T cells. Immunoprecipitation was performed with GFP (*A*) or Flag (*B*) antibodies. *C*, His pulldown assay revealing the *in vitro* interaction between His-stathmin and GST-PKG1. *D*, immunoprecipitation and immunoblotting results showing the interaction of endogenous PKG1 with stathmin in intestinal, oral, and vaginal epithelial cells. *E*, immunoprecipitation and immunoblotting results showing the phosphorylation of stathmin-GFP in Ca9-22 cells transfected with indicated concentrations of PKG1-Flag and treated with gp120. *F*, human stathmin phosphotarget map showing S38 and S63 relative to other known phosphorylation sites. *G* and *H*, immunoblot analysis of stathmin, p-S63-stathmin, and p-S38-stathmin in RKO cells treated with HIV-1 for 24 h (*G*) and with 1 μg/mL gp120 for the indicated time (*H*). *I* and *J*, immunoblot analysis of stathmin, p-S63-stathmin, and PKG1 or PKA in RKO cells treated with gp120 for 24 h after PKG1 or PKA knockdown.

phosphorylation interferes with the stability of stathmin. Treatment of cells with HIV-1 gp120 activated PKG1 and further increased stathmin serine/threonine phosphorylation, while markedly reducing stathmin protein levels (Fig. 3*E*).

Liquid chromatography–tandem mass spectrometry (LC-MS/MS) analysis identified serine 38 and 63 as the residues in stathmin that were phosphorylated upon HIV-1 gp120 treatment (Fig. 3*F*, Fig. S1, *A* and *B*, and Table S2). Using phosphorylation-specific antibodies, we found that serine 63 phosphorylation was increased in Caco-2 cells exposed to HIV-1 pseudoviruses or treated with gp120, while serine 38 phosphorylation was not obviously affected (Fig. 3, *G* and *H*). Treatment of cells with Rp-8-pCPT-cyclic GMPS sodium (RPG), an inhibitor of PKG1 activity (29), abrogated the increase in stathmin serine 63 phosphorylation (Fig. S2*A*). Moreover, siRNA-mediated PKG1 depletion could also block the increase in serine 63 phosphorylation and degradation of stathmin (Fig. 3*I*). As protein kinase A (PKA) could also phosphorylate stathmin at serine 63, we carried out PKA knockdown (Fig. 3*J*) or inhibition of its activity with H-89 (Fig. S2*B*) and found that PKA depletion could not abrogate the increase of serine 63 phosphorylation and degradation of stathmin. In addition, PKA depletion did not abrogate the decrease in junctional localization of ZO-1 and E-cadherin under HIV-1 gp120 treatment (Fig. S3, *A*–*D*). These results indicate that interaction with PKG1 promotes stathmin serine 63 phosphorylation and that this is enhanced upon HIV-1 exposure.

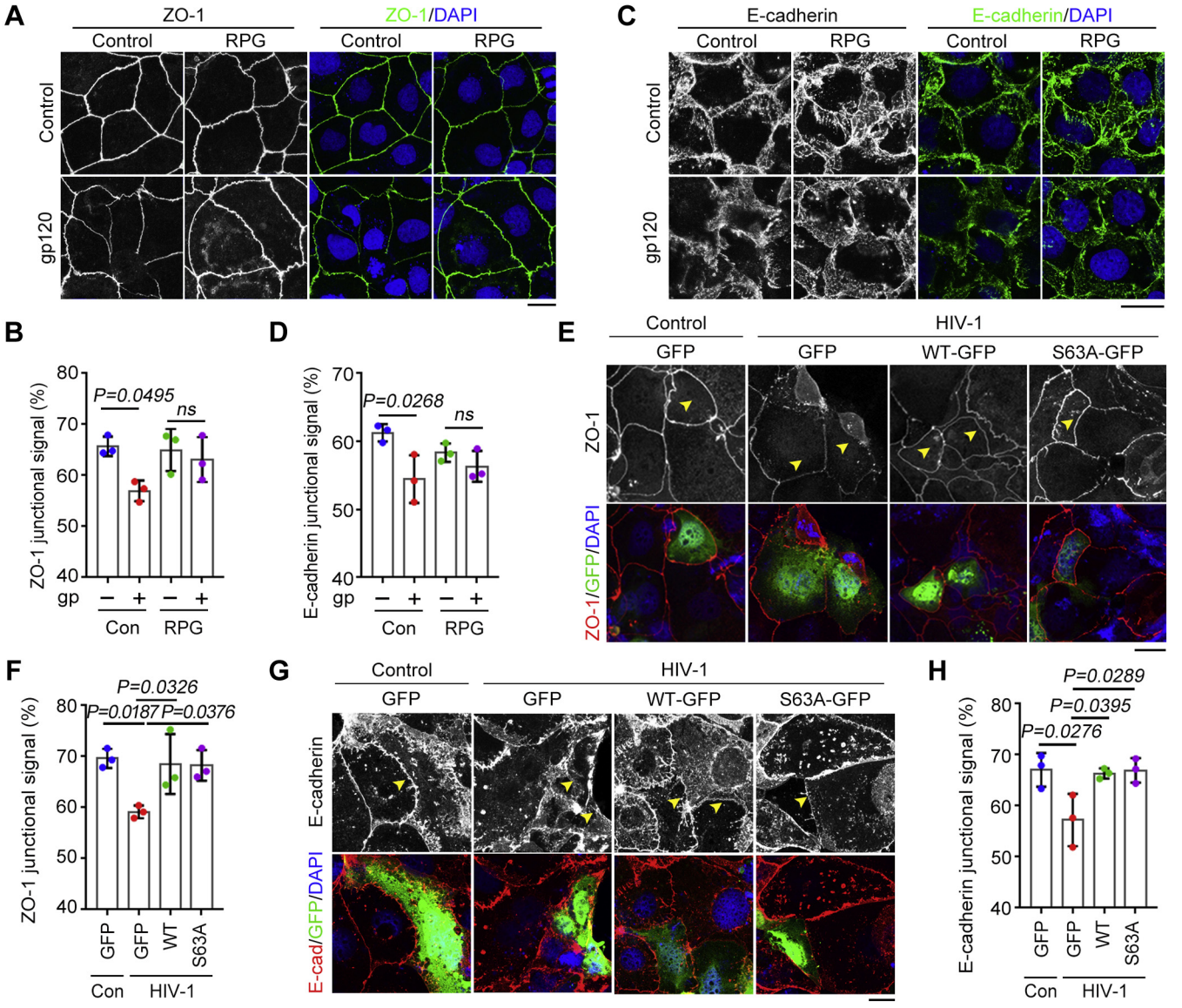

Figure 4. PKG1-mediated stathmin phosphorylation leads to perturbation of cell junctions upon HIV-1 exposure. *A* and *C*, immunofluorescence labeling of ZO-1 (*A*) and E-cadherin (*C*) in cells treated with gp120 and RPG (20 μM). Scale bars, 25 μm. *B* and *D*, quantification of the fluorescence intensity of ZO-1 (*B*) and E-cadherin (*D*) at cell junctions. $n = 3$ biological replicates. *E* and *G*, immunofluorescence labeling of ZO-1 (*E*) and E-cadherin (*G*) in Caco-2 cells transfected with GFP vector, WT stathmin-GFP, or S63A stathmin-GFP for 24 h followed by treatment with HIV-1 for 24 h. Scale bars, 20 μm. *F* and *H*, quantification of ZO-1 (*F*) and E-cadherin (*H*) fluorescence intensity at cell junctions. $n = 3$ biological replicates. Data are presented as mean ± SD. ns, not significant.

PKG1-mediated stathmin phosphorylation underlies the disruption of cell junctions by HIV-1

The pathological link between stathmin phosphorylation by PKG1 and the disruption of cell junctions by HIV-1 is supported by our observation that PKG1 knockdown rescued the junctional damage caused by HIV-1 gp120 treatment (Fig. 2, *E–H*). Based on these data, we investigated whether inhibition of PKG1 activity would rescue this junctional breakdown. As expected, treatment with the PKG1 inhibitor RPG mitigated HIV-1 gp120-induced loss of junctional integrity, including that of tight junctions (Fig. 4, *A* and *B*) and adherens junctions (Fig. 4, *C* and *D*). We next assessed the integrity of cell junctions in the presence or absence of HIV-1 with stathmin overexpression/rescue experiments in Caco-2 cells. HIV-1-disrupted cell junctions could be rescued by overexpression of stathmin-GFP (Fig. 4, *E–H*). However, mutation of the stathmin serine 63 residue phosphorylated by PKG1 restored junctional integrity much better. Thus, HIV-1-induced epithelial junction damage is directly related to PKG1-mediated stathmin phosphorylation.

The PKG1/Stathmin axis modulates HIV-1-induced microtubule hyperstabilization

The tubulin-binding capacity of stathmin is reduced and the microtubule-depolymerization function of stathmin is inhibited by its phosphorylation at serine 63 (27). We tested whether the PKG1/stathmin signaling axis mediates stathmin-dependent changes in microtubule stability induced by HIV-1 exposure. In addition to restoring cell junctions, PKG1 knockdown abolished the microtubule-hyperstabilizing effects of HIV-1 gp120 (Fig. 5, *A* and *B*), confirming the essential role of PKG1 in HIV-1-induced microtubule hyperstabilization.

Application of the microtubule-depolymerizing agent nocodazole to disrupt bundled microtubules reversed the damage to tight and adherens junctions caused by HIV-1 gp120 (Fig. 5, *C–E*), suggesting that the junctional disruption was caused by PKG1/stathmin-mediated microtubule hyperstabilization. To evaluate this possibility, stathmin was overexpressed in cells with or without HIV-1 exposure, and microtubule morphology was analyzed. Overexpression of stathmin-GFP abrogated HIV-1-induced microtubule hyperstabilization, and this effect was enhanced when the stathmin S63A (phosphodeficient) mutant was overexpressed (Fig. 5, *F* and *G*). Thus, PKG1-mediated stathmin phosphorylation underlies the microtubule hyperstabilization induced by HIV-1.

Stathmin phosphorylation at serine 63 promotes its autophagic degradation

Our previous work showed that stathmin was targeted for autophagic degradation by treatment with HIV-1 gp120 (17). Overexpression of PKG1 decreased stathmin protein levels (Fig. 3*E*), whereas PKG1 depletion had the opposite effect (Fig. 3*I*). We examined the relationship between stathmin phosphorylation and autophagic degradation in greater detail by comparing the half-lives of WT, S63A (phosphodeficient) mutant, and S63D (phosphomimetic) mutant stathmin-GFP proteins. The S63A and S63D mutants had longer and shorter half-lives, respectively, than WT stathmin (Fig. 6, *A* and *B*), indicating that stathmin phosphorylation at serine 63 decreases its stability.

Autophagosomes can be visualized by detection of fluorescently labeled microtubule-associated protein 1A/1B-light chain 3 (LC3) puncta (30, 31). We examined the intracellular distribution of WT, S63A, and S63D stathmin-GFP proteins. We found that more S63D stathmin was targeted to intracellular LC3 puncta compared with the WT protein following gp120 treatment (Fig. 6*C*). To investigate the underlying mechanism, we analyzed the domain of stathmin that interacts with p62 using a set of stathmin deletion mutants fused to GFP (Fig. 6*D*). Immunoprecipitation experiments showed that p62 interacted with different domains of stathmin, but much less with the N-terminal truncation mutant (Fig. 6*E*). Moreover, less S63A and more S63D stathmin-GFP coprecipitated with Flag-p62 compared with the WT protein (Fig. 6*F*). These results indicate that PKG1-mediated phosphorylation of stathmin at serine 63 promotes stathmin degradation by autophagy.

Discussion

The binding of HIV-1 gp120 to its chemokine coreceptor CCR5 or CXCR4 is known to trigger the activation of multiple signaling pathways related to the pathogenesis of HIV-1 infection (32–35). The results presented here reveal the molecular mechanism by which HIV-1 penetrates the epithelial barrier as well as the pathological significance of this novel regulatory pathway (Fig. 6*G*). HIV-1 exposure triggers PKG1 activation and stathmin phosphorylation, inhibition, and degradation, leading to the hyperstabilization of microtubules and disruption of epithelial cell junctions (Fig. 6*G*). The gp120 protein is the major focus of developing HIV-1 vaccines (36). Efforts to develop HIV-1 vaccines targeting gp120, however, have been hampered by the chemical and structural properties of gp120, which make it difficult for antibody binding. The present study provides novel insights into the molecular mechanisms of HIV-1-induced mucosal barrier dysfunction, which may facilitate the development of vaccines targeting gp120.

Stathmin functions as an intracellular relay for multiple regulatory pathways (37–39). Stathmin phosphorylation is known to modulate the microtubule architecture (24, 26). For example, phosphorylation by the Epstein-Barr virus kinase BGLF4 at serine 16, 25, and 38 reduces the microtubule-destabilizing capacity of stathmin (40). Our results reveal that stathmin phosphorylation at serine 63 is markedly increased upon HIV-1 exposure. Serine 63 phosphorylation by PKA is known to inhibit stathmin activity and promote microtubule depolymerization (41). We have sought to identify the role of PKA in stathmin phosphorylation induced by HIV-1 gp120. Our data show that PKA depletion could not block the induction of stathmin phosphorylation, although PKA knockdown could indeed decrease the basal level of stathmin phosphorylation. In this study, we have identified PKG1 by LC-MS/MS analysis as a novel kinase of stathmin that

specifically phosphorylates the serine 63 residue in the presence of HIV-1 pseudoviruses or recombinant gp120 protein. PKG1 acts as serine/threonine kinase that protects against heart disease, neuronal disease, and thoracic aortic disease. Serine 27, serine 45, serine 51, threonine 59, serine 65, serine 73, and threonine 85 residues of PKG1 have been reported to undergo autophosphorylation *in vitro* (42). We provide evidence that the phosphorylation of PKG1 is increased by gp120 treatment. We speculate that PKG1 may be activated through autophosphorylation upon gp120 treatment and then phosphorylate stathmin at serine 63. These findings indicate that the inhibition of stathmin activity by PKG1-mediated phosphorylation contributes to HIV-1-induced microtubule hyperstabilization.

Binding of gp120 to its chemokine coreceptor CCR5 or CXCR4 is known to trigger the activation of multiple signaling pathways related to HIV-1 pathogenesis (32–35). Autophagy is critically involved in the defense against viral infection and antiviral immune responses. It has been demonstrated that autophagy is induced by various pathogens, such as HIV-1, herpes simplex virus type 1, and hepatitis C virus, implicating autophagy as a potential antiviral target. HIV-1 Tat is shown to induce autophagy in neuroblastoma cells (43). The interaction of gp120 with CXCR4 has been reported to mediate HIV-1 Env-mediated autophagy (35). PKG1, as a key mediator of nitric oxide signaling, has been shown to induce autophagy through phosphorylating tuberous sclerosis complex 2 (TSC2) (44). These findings, together with our observation that stathmin phosphorylation by PKG1 results in autophagic degradation of stathmin, suggest a complex regulation of protein levels by autophagy upon HIV-1 infection. It is tempting to speculate that, at the early stage of HIV-1 transmission, gp120 may trigger autophagy in the epithelium *via* activation of the PKG1/TSC2 axis. Further studies are warranted to test this possibility. In addition to gp120, gp41, another glycoprotein of the HIV-1 envelope, has been shown to mediate HIV-1 envelope-induced autophagy *via* its fusogenic function in uninfected bystander CD4+ T cells (45). The recombinant gp120 used in our study contains the N-terminal heptad repeat and C-terminal heptad repeat domains of gp41 but does not contain its fusion peptide, largely excluding the involvement of gp41 in HIV-1-induced autophagy.

Our findings have important implications for the prevention of sexual transmission of HIV-1 because they indicate that HIV-1-induced disruption of epithelial cell junctions can be effectively abrogated by pharmacological inhibition of PKG1 activity. Additional studies are needed to determine whether specifically targeting stathmin phosphorylation, microtubule

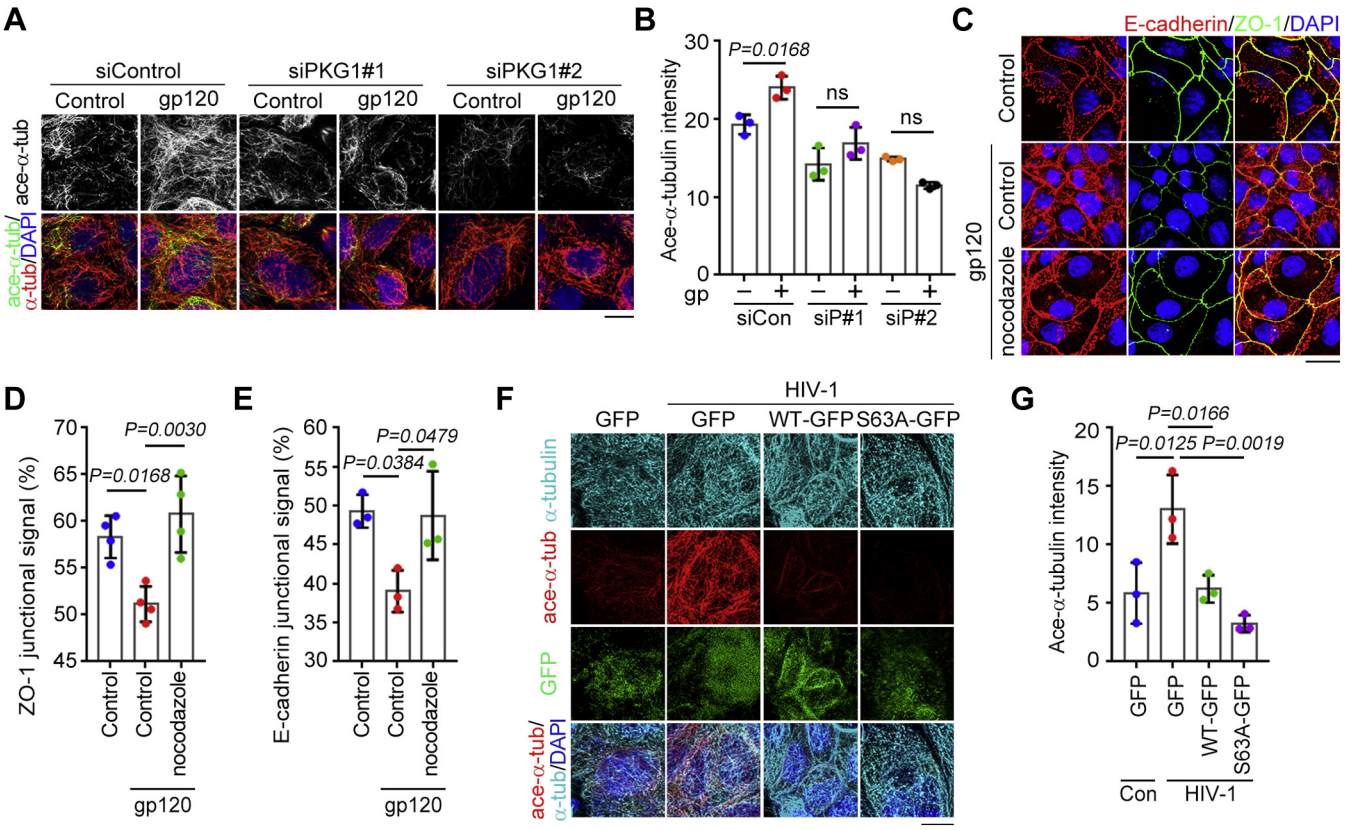

Figure 5. The PKG1/stathmin axis mediates microtubule hyperstabilization upon HIV-1 exposure. *A*, immunofluorescence labeling of α-tubulin and acetylated α-tubulin in cells treated with gp120 for 24 h following PKG1 knockdown. Scale bar, 10 μm. *B*, quantification of acetylated α-tubulin fluorescence. $n = 3$ biological replicates. *C*, immunofluorescence labeling of ZO-1 and E-cadherin in cells treated with gp120 for 24 h; 10 μM nocodazole was added for the last hour. Scale bar, 25 μm. *D*, quantification of ZO-1 fluorescence intensity. $n = 4$ biological replicates. *E*, quantification of E-cadherin fluorescence intensity. $n = 3$ biological replicates. *F*, immunofluorescence labeling of α-tubulin and acetylated α-tubulin in Caco-2 cells transfected with GFP vector, WT stathmin-GFP, or S63A stathmin-GFP for 24 h followed by HIV-1 treatment. Scale bar, 20 μm. *G*, quantification of acetylated α-tubulin fluorescence. $n = 3$ biological replicates. Data are presented as mean ± SD. ns, not significant.

dynamics (46, 47), or junctional complex formation can alleviate the effect of HIV-1 on epithelial cell junctions. Moreover, elucidating the molecular mechanisms underlying the earliest stages of HIV-1 infection can guide the development of effective vaccines and microbicides that block HIV-1 transmission and prevent systemic infection and associated pathologies.

Experimental procedures

Cell culture and transfection

Caco-2 and RKO human epithelial cell lines were cultured in Minimal Essential Medium (Thermo Fisher Scientific). HEK293T human embryonic kidney cells were cultured in Dulbecco's Modified Eagle's Medium (Hyclone). All cells were cultured in medium supplemented with 10% to 20% fetal bovine serum and penicillin/streptomycin (100 U/mL, both from Biological Industries) at 37 °C in a humidified incubator of 5% CO_2. AMD3100, chloroquine, 4',6-diamidino-2-phenylindole (DAPI), and bafilomycin A1 were purchased from Sigma-Aldrich; H-89 was from MedChemExpress; and RPG was from Santa Cruz Biotechnology. Cell transfection was performed as described (17, 48).

Generation of pseudotyped HIV-1

Env-pseudotyped HIV-1 and VSVG-pseudotyped control viruses were obtained by cotransfecting HEK293T cells with NLENY1-ES-IRES encoding the HIV-1 backbone (provided by Dr David Levy, University of Alabama at Birmingham), along

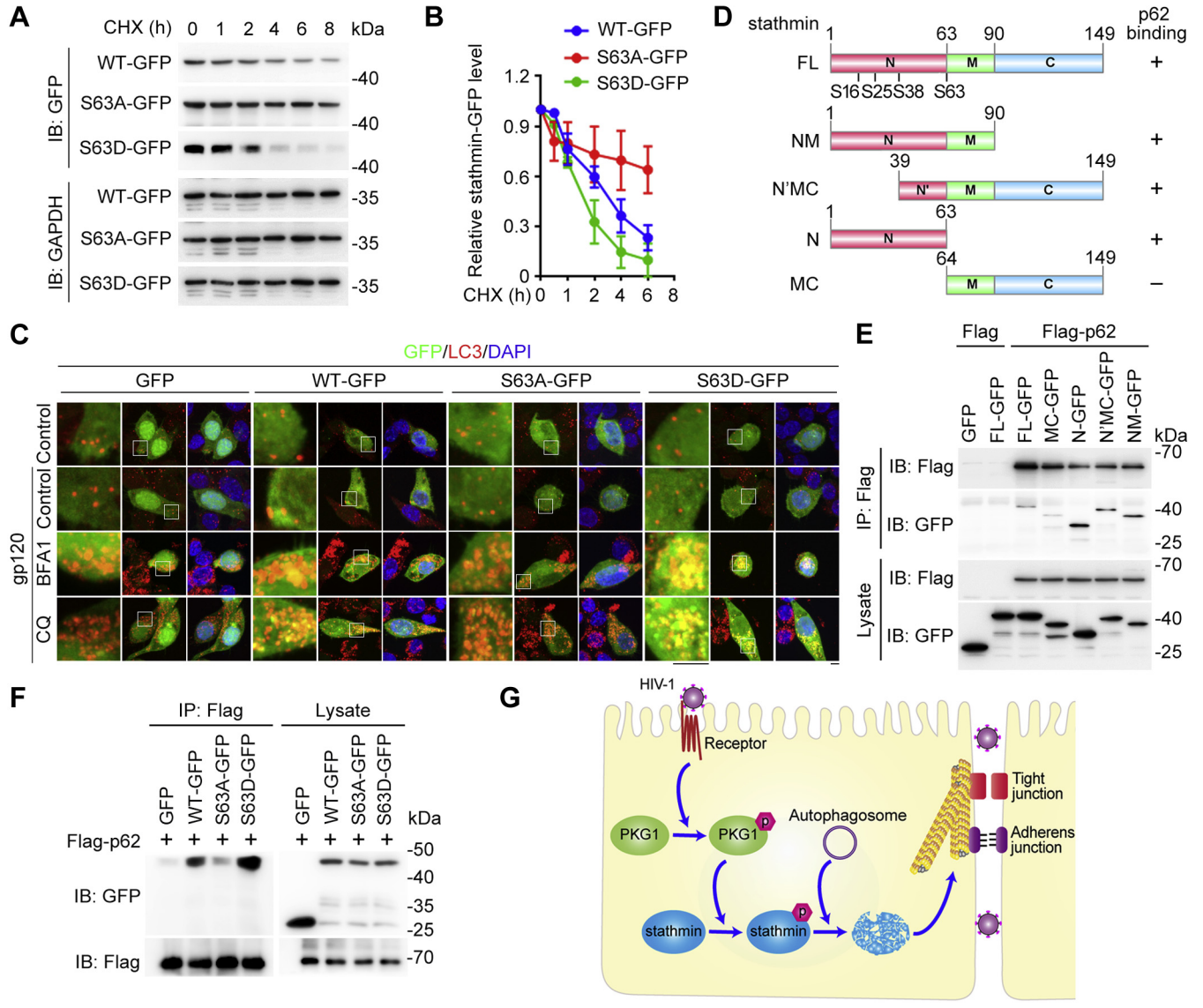

Figure 6. PKG1-mediated phosphorylation promotes stathmin degradation *via* autophagy. *A*, immunoblot analysis of wildtype (WT) and S63A and S63D stathmin-GFP expression in cells treated with 100 μg/mL cycloheximide (CHX) for the indicated time. *B*, quantification of WT, S63A, and S63D stathmin-GFP levels. $n = 3$ biological replicates. *C*, colocalization of LC3 puncta with WT or S63A or S63D stathmin-GFP in cells treated with gp120 and 100 nM bafilomycin A1 (BFA1) or 25 μM chloroquine (CQ) for 24 h. Scale bars, 5 μm. *D*, schematic illustration of stathmin deletion mutants. *E* and *F*, immunoprecipitation and immunoblotting results showing the interaction of Flag-p62 with stathmin-GFP deletion mutants (*E*) and with WT, S63A, or S63D stathmin-GFP (*F*) in HEK293T cells. *G*, model of HIV-1-induced microtubule hyperstabilization *via* the PKG1/stathmin axis.

with pSRHS-Env (provided by Dr Eric Hunter, Emory University), or pVSVG (provided by Dr David Levy), respectively, as described (49). The supernatant was collected 48 h after transfection. To determine the viral titer, harvested viruses were used to infect TZM-bl reporter cells and the luciferase assay was performed using a GloMax luminometer (Promega) (49).

Plasmids, siRNAs, and purified proteins

Stathmin and p62 cDNAs were amplified by PCR and cloned into the pEGFP-N1 and pCMV5-Flag vectors, respectively. pCMV6-Flag-PKG1 was obtained from OriGene. Stathmin deletion and point mutants were generated using the QuikChange Site-Directed Mutagenesis kit (Stratagene). siPKA (5'-CAAGGACAACUCAAACUUA-3'), siPKG1 (#1: 5'-CACCGAGUGAAGACCCAGU-3' and #2: 5'-GGAUA GAGGUUCGUUUGAA-3'), and siADCK3 (#1: 5'-CGGGAC AAGUUGGAAUACU-3' and #2: 5'-GGGCUCAGCCAGGA GAUUC-3') were synthesized by RiboBio. Recombinant HIV-1 gp120 was expressed in stably transfected *Drosophila* S2 cells and purified by affinity chromatography followed by size exclusion chromatography, as described (50).

Mass spectrometry

To identify proteins interacting with stathmin-GFP, the immunoprecipitated proteins bound to GFP-beads were subjected to mass spectrometry by Lu-Ming Biotech Co. To identify stathmin-GFP phosphorylation sites under HIV-1 gp120 treatment, the immunoprecipitated proteins bound to GFP-beads were subjected to Coomassie blue staining and mass spectrometry by PTM Biolabs. The eluted proteins from the immunoprecipitation assay were identified using a gel-based LC-MS approach. The data processing was conducted using the Q-Exactive or Orbitrap Elite mass spectrometer (Thermo Fisher Scientific). In the mass spectrometry, Thermo Proteome Discoverer 2.1 was used as the peaklist-generating software and the search engine. The sequence database searched was homo sapiens (Homo_sapiens_9606_Swiss-Prot). The number of entries in the database actually searched was 20,365. Trypsin/P was specified as the cleavage enzyme to generate peptides. The number of missed and/or nonspecific cleavages permitted was two. Carbamidomethyl on Cys were specified as fixed modification. Oxidation (Met), acetyl (Protein N-term), and deamidated (NQ) were specified as variable modifications. Mass tolerance for precursor ions was set to 10 ppm. Mass tolerance for fragment ions was set to 0.05 Da. Peptide confidence was set at high, and peptide ion score was set >20. The false discovery rate (FDR) was <1%. The FDR was calculated (for large datasets) as follows: The protein database used in the search database was called the positive library, and all protein sequences were reversed as the antilibrary. If a peptide sequence could be attributed to both the positive and the antilibrary, it would not be trusted. The probability of a peptide going to the reverse library (the FDR value) was required to be less than 1%.

Immunoprecipitation and immunoblotting

Total cell lysates were extracted in boiling sodium dodecyl sulfate (SDS) sample buffer. Immunoprecipitation lysates were prepared with Triton X-100 lysis buffer (50 mM Tris-HCl [pH 7.4], 150 mM NaCl, 1 mM Na_4VO_3, 10 mM NaF, 1 mM EDTA, and 1% Triton X-100) supplemented with phenylmethylsulfonyl fluoride (1 mM) and protease inhibitor cocktail (Roche Diagnostics). Proteins were separated by SDS–polyacrylamide gel electrophoresis and transferred to a polyvinylidene difluoride membrane (Merck Millipore) that was incubated overnight at 4 °C with primary antibodies and then probed with horseradish peroxidase (HRP)-conjugated secondary antibodies. Chemiluminescence detection was performed with Western HRP substrate (Merck Millipore). Immunoprecipitation, His pulldown, and coimmunoprecipitation assays were performed as described (17). Primary antibodies against the following proteins were used: acetylated α-tubulin (Merck Millipore; Sigma-Aldrich); α-tubulin, stathmin, phospho(p)-S63-stathmin, p-Ser/Thr, PKG1, and E-cadherin (all from Abcam); stathmin and PKG1 (both from Proteintech); pTyr, β-actin, GFP, and Flag (Abways); p62 and LC3 (MBL); and ZO-1 (Thermo Fisher Scientific). HRP-conjugated secondary antibodies were from Amersham Biosciences. Protein A/G-agarose (Pierce), GFP-agarose (MBL), and Flag-agarose (Abmart) beads were used for immunoprecipitation.

Immunofluorescence analysis

The expression and localization of specific proteins were detected by immunofluorescence labeling. Briefly, fixed cells were blocked with 4% bovine serum albumin for 1 h and incubated overnight at 4 °C with primary antibodies followed by Alexa Fluor 488- or 568-conjugated secondary antibodies (Abcam) at room temperature in the dark for 1 h. DAPI was used to stain cell nuclei, and samples and coverslips were mounted with 90% glycerol in phosphate-buffered saline. The slides were observed with a fluorescence microscope (Leica) or a laser confocal microscope (Leica) to obtain a *z*-axis scan. The polyhedral tool of ImageJ software (National Institutes of Health) was used to quantify fluorescence. The fluorescence intensity of the samples was determined by subtracting background signal. The signal (%) of different junctional markers was calculated as the ratio of fluorescence intensity in the junction area to that in the whole cell as described (51).

Statistical analysis

All statistical comparisons were performed using Prism software (GraphPad). Data are expressed as mean ± SD and were analyzed with the unpaired two-tailed *t* test or by one-way analysis of variance. $p < 0.05$ was considered statistically significant.

Data availability

The mass spectrometry proteomics data have been deposited to the ProteomeXchange Consortium *via* the PRIDE (52)

partner repository (http://www.ebi.ac.uk/pride) with the dataset identifier PXD023868 and PXD023906.

Supporting information—This article contains supporting information.

Acknowledgments—This work was supported by grants from the National Key R&D Program of China [2018YFA0107001] and the National Natural Science Foundation of China [31701209 and 31471262].

Author contributions—W. X., J. Z., and M. L. conceptualization; W. X., D. L., J. Z., and M. L. software; W. X., J. Z., and M. L. supervision; W. X. and Z. J. funding acquisition; W. X., M. C., Z. Z., H. L., T. S., Y. Z., D. D., P. Z., and Y. Z. investigation; W. X., L. D., Y. Z., J. Z., and M. L. methodology; W. X. and J. Z. writing—original draft; W. X., D. L., J. Z., and M. L. project administration; W. X., J. Z., and M. L. writing—review and editing; M. C., Z. Z., H. L., and Y. Z. validation; L. D., Y. Z., X. L., and M. L. resources; and J. Z. data curation.

Conflict of interest—The authors declare that they have no conflicts of interest with the contents of this article.

Abbreviations—The abbreviations used are: ADCK3, AarF domain-containing kinase 3; CAMSAP3, calmodulin-regulated spectrin-associated protein 3; CCR5, C-C chemokine receptor type 5; CD4, cluster of differentiation 4; CXCR4, C-X-C chemokine receptor type 4; FDR, false discovery rate; HRP, horseradish peroxidase; LC3, light chain 3; PKG1, protein kinase G 1; PLEKHA7, pleckstrin homology domain-containing A7; RPG, Rp-8-pCPT-cyclic GMPS sodium; TSC2, tuberous sclerosis complex 2; VSVG, vesicular stomatitis virus glycoprotein; ZO-1, zona occludens 1.

References

1. Hladik, F., and McElrath, M. J. (2008) Setting the stage: Host invasion by HIV. *Nat. Rev. Immunol.* **8**, 447–457
2. Nazli, A., Chan, O., Dobson-Belaire, W. N., Ouellet, M., Tremblay, M. J., Gray-Owen, S. D., Arsenault, A. L., and Kaushic, C. (2010) Exposure to HIV-1 directly impairs mucosal epithelial barrier integrity allowing microbial translocation. *PLoS Pathog.* **6**, e1000852
3. Tugizov, S. (2016) Human immunodeficiency virus-associated disruption of mucosal barriers and its role in HIV transmission and pathogenesis of HIV/AIDS disease. *Tissue Barriers* **4**, e1159276
4. Cicala, C., Nawaz, F., Jelicic, K., Arthos, J., and Fauci, A. S. (2016) HIV-1 gp120: A target for therapeutics and vaccine design. *Curr. Drug Targets* **17**, 122–135
5. Haase, A. T. (2010) Targeting early infection to prevent HIV-1 mucosal transmission. *Nature* **464**, 217–223
6. Shaik, M. M., Peng, H., Lu, J., Rits-Volloch, S., Xu, C., Liao, M., and Chen, B. (2018) Structural basis of coreceptor recognition by HIV-1 envelope spike. *Nature* **565**, 318–323
7. France, M. M., and Turner, J. R. (2017) The mucosal barrier at a glance. *J. Cell Sci.* **130**, 307–314
8. Dong, D., Xie, W., and Liu, M. (2020) Alteration of cell junctions during viral infection. *Thorac. Cancer* **11**, 519–525
9. Yang, Y., and Zhou, J. (2016) Cyld - a deubiquitylase that acts to fine-tune microtubule properties and functions. *J. Cell Sci.* **129**, 2289–2295
10. Basu, R., Bose, A., Thomas, D., and Das Sarma, J. (2017) Microtubule-assisted altered trafficking of astrocytic gap junction protein connexin 43 is associated with depletion of connexin 47 during mouse hepatitis virus infection. *J. Biol. Chem.* **292**, 14747–14763
11. Xie, W., Yang, Y., Gao, S., Song, T., Wu, Y., Li, D., Liu, M., and Zhou, J. (2017) The tumor suppressor CYLD controls epithelial morphogenesis and homeostasis by regulating mitotic spindle behavior and adherens junction assembly. *J. Genet. Genomics* **44**, 343–353
12. Yano, T., Matsui, T., Tamura, A., Uji, M., and Tsukita, S. (2013) The association of microtubules with tight junctions is promoted by cingulin phosphorylation by AMPK. *J. Cell Biol.* **203**, 605–614
13. Gavilan, M. P., Arjona, M., Zurbano, A., Formstecher, E., Martinez-Morales, J. R., Bornens, M., and Rios, R. M. (2015) Alpha-catenin-dependent recruitment of the centrosomal protein CAP350 to adherens junctions allows epithelial cells to acquire a columnar shape. *PLoS Biol.* **13**, e1002087
14. Meng, W., Mushika, Y., Ichii, T., and Takeichi, M. (2008) Anchorage of microtubule minus ends to adherens junctions regulates epithelial cell-cell contacts. *Cell* **135**, 948–959
15. Vasileva, E., and Citi, S. (2018) The role of microtubules in the regulation of epithelial junctions. *Tissue Barriers* **6**, 1539596
16. Paschoud, S., Jond, L., Guerrera, D., and Citi, S. (2014) PLEKHA7 modulates epithelial tight junction barrier function. *Tissue Barriers* **2**, e28755
17. Xie, W., Li, D., Dong, D., Li, Y., Zhang, Y., Duan, L., Liu, X., Meng, W., Liu, M., and Zhou, J. (2020) HIV-1 exposure triggers autophagic degradation of stathmin and hyperstabilization of microtubules to disrupt epithelial cell junctions. *Signal Transduct. Target. Ther.* **5**, 79
18. Garcia, M. A., Nelson, W. J., and Chavez, N. (2018) Cell-cell junctions organize structural and signaling networks. *Cold Spring Harb. Perspect. Biol.* **10**, a029181
19. Sun, S., and Zhou, J. (2020) Phase separation as a therapeutic target in tight junction-associated human diseases. *Acta Pharmacol. Sin.* **41**, 1310–1313
20. Angulo-Urarte, A., van der Wal, T., and Huveneers, S. (2020) Cell-cell junctions as sensors and transducers of mechanical forces. *Biochim. Biophys. Acta* **1862**, 183316
21. De Clercq, E. (2015) AMD3100/CXCR4 inhibitor. *Front. Immunol.* **6**, 276
22. Yang, Y., Chen, M., Li, J., Hong, R., Yang, J., Yu, F., Li, T., Yang, S., Ran, J., Guo, C., Zhao, Y., Luan, Y., Liu, M., Li, D., Xie, S., *et al.* (2020) A cilium-independent role for intraflagellar transport 88 in regulating angiogenesis. *Sci. Bull.* **66**, 727–739
23. Eshun-Wilson, L., Zhang, R., Portran, D., Nachury, M. V., Toso, D. B., Lohr, T., Vendruscolo, M., Bonomi, M., Fraser, J. S., and Nogales, E. (2019) Effects of alpha-tubulin acetylation on microtubule structure and stability. *Proc. Natl. Acad. Sci. U. S. A.* **116**, 10366–10371
24. Belmont, L. D., and Mitchison, T. J. (1996) Identification of a protein that interacts with tubulin dimers and increases the catastrophe rate of microtubules. *Cell* **84**, 623–631
25. Cassimeris, L. (2002) The oncoprotein 18/stathmin family of microtubule destabilizers. *Curr. Opin. Cell Biol.* **14**, 18–24
26. Marklund, U., Larsson, N., Gradin, H., Brattsand, G., and Gullberg, M. (1996) Oncoprotein 18 is a phosphorylation-responsive regulator of microtubule dynamics. *EMBO J.* **15**, 5290–5298
27. Manna, T., Thrower, D. A., Honnappa, S., Steinmetz, M. O., and Wilson, L. (2009) Regulation of microtubule dynamic instability *in vitro* by differentially phosphorylated stathmin. *J. Biol. Chem.* **284**, 15640–15649
28. Beretta, L., Dobransky, T., and Sobel, A. (1993) Multiple phosphorylation of stathmin. Identification of four sites phosphorylated in intact cells and *in vitro* by cyclic AMP-dependent protein kinase and p34cdc2. *J. Biol. Chem.* **268**, 20076–20084
29. Butt, E., Eigenthaler, M., and Genieser, H.-G. (1994) (Rp)-8-pCPT-cGMPS, a novel cGMP-dependent protein kinase inhibitor. *Eur. J. Pharmacol. Mol. Pharmacol.* **269**, 265–268
30. Yoshii, S. R., and Mizushima, N. (2017) Monitoring and measuring autophagy. *Int. J. Mol. Sci.* **18**, 1865
31. Xie, W., and Zhou, J. (2018) Aberrant regulation of autophagy in mammalian diseases. *Biol. Lett.* **14**, 20170540
32. Nazli, A., Kafka, J. K., Ferreira, V. H., Anipindi, V., Mueller, K., Osborne, B. J., Dizzell, S., Chauvin, S., Mian, M. F., Ouellet, M., Tremblay, M. J., Mossman, K. L., Ashkar, A. A., Kovacs, C., Bowdish, D. M., *et al.* (2013)

HIV-1 gp120 induces TLR2- and TLR4-mediated innate immune activation in human female genital epithelium. *J. Immunol.* **191**, 4246–4258
33. Liu, Z., Qiao, L., Zhang, Y., Zang, Y., Shi, Y., Liu, K., Zhang, X., Lu, X., Yuan, L., Su, B., Zhang, T., Wu, H., and Chen, D. (2017) ASPP2 plays a dual role in gp120-induced autophagy and apoptosis of neuroblastoma cells. *Front. Neurosci.* **11**, 150
34. Melar, M., Ott, D. E., and Hope, T. J. (2007) Physiological levels of virion-associated human immunodeficiency virus type 1 envelope induce coreceptor-dependent calcium flux. *J. Virol.* **81**, 1773–1785
35. Espert, L., Denizot, M., Grimaldi, M., Robert-Hebmann, V., Gay, B., Varbanov, M., Codogno, P., and Biard-Piechaczyk, M. (2006) Autophagy is involved in T cell death after binding of HIV-1 envelope proteins to CXCR4. *J. Clin. Invest.* **116**, 2161–2172
36. Beena, V., Choudhary, K., Rajeev, R., Sivakumar, R., Heera, R., and Padmakumar, S. (2013) Human immunodeficiency virus vaccine an update. *J. Oral Maxillofac. Pathol.* **17**, 76–81
37. Xu, K., and Harrison, R. E. (2015) Down-regulation of stathmin is required for the phenotypic changes and classical activation of macrophages. *J. Biol. Chem.* **290**, 19245–19260
38. Lu, N. T., Liu, N. M., Patel, D., Vu, J. Q., Liu, L., Kim, C. Y., Cho, P., Khachatoorian, R., Patel, N., Magyar, C. E., Ganapathy, E., Arumugaswami, V., Dasgupta, A., and French, S. W. (2018) Oncoprotein stathmin modulates sensitivity to apoptosis in hepatocellular carcinoma cells during Hepatitis C viral replication. *J. Cell Death* **11**, 1179066018785141
39. Lin, X., Liao, Y., Chen, X., Long, D., Yu, T., and Shen, F. (2016) Regulation of oncoprotein 18/stathmin signaling by ERK concerns the resistance to taxol in nonsmall cell lung cancer cells. *Cancer Biother. Radiopharm.* **31**, 37–43
40. Chen, P. W., Lin, S. J., Tsai, S. C., Lin, J. H., Chen, M. R., Wang, J. T., Lee, C. P., and Tsai, C. H. (2010) Regulation of microtubule dynamics through phosphorylation on stathmin by Epstein-Barr virus kinase BGLF4. *J. Biol. Chem.* **285**, 10053–10063
41. Yip, Y. Y., Yeap, Y. Y., Bogoyevitch, M. A., and Ng, D. C. (2014) cAMP-Dependent protein kinase and c-Jun N-terminal kinase mediate stathmin phosphorylation for the maintenance of interphase microtubules during osmotic stress. *J. Biol. Chem.* **289**, 2157–2169
42. Pinkse, M. W. H., Heck, A. J. R., Rumpel, K., and Pullen, F. (2004) Probing noncovalent protein-ligand interactions of the cGMP-dependent protein kinase using electrospray ionization time of flight mass spectrometry. *J. Am. Soc. Mass Spectrom.* **15**, 1392–1399
43. Li, J., Wang, W., Tong, P., Leung, C. K., Yang, G., Li, Z., Li, N., Sun, X., Han, Y., Lu, C., Kuang, D., Dai, J., and Zeng, X. (2018) Autophagy induction by HIV-tat and methamphetamine in primary midbrain neuronal cells of tree shrews via the mTOR signaling and ATG5/ATG7 pathway. *Front. Neurosci.* **12**, 921
44. Ranek, M. J., Kokkonen-Simon, K. M., Chen, A., Dunkerly-Eyring, B. L., Vera, M. P., Oeing, C. U., Patel, C. H., Nakamura, T., Zhu, G., Bedja, D., Sasaki, M., Holewinski, R. J., Van Eyk, J. E., Powell, J. D., Lee, D. I., *et al.* (2019) PKG1-modified TSC2 regulates mTORC1 activity to counter adverse cardiac stress. *Nature* **566**, 264–269
45. Denizot, M., Varbanov, M., Espert, L., Robert-Hebmann, V., Sagnier, S., Garcia, E., Curriu, M., Mamoun, R., Blanco, J., and Biard-Piechaczyk, M. (2008) HIV-1 gp41 fusogenic function triggers autophagy in uninfected cells. *Autophagy* **4**, 998–1008
46. Liu, M., Du, X., and Zhou, J. (2018) Non-canonical function of Tat in regulating host microtubule dynamics: Implications for the pathogenesis of lentiviral infections. *Pharmacol. Ther.* **182**, 28–32
47. Chen, M., Wang, J., Yang, Y., Zhong, T., Zhou, P., Ma, H., Li, J., Li, D., Zhou, J., Xie, S., and Liu, M. (2020) Redox-dependent regulation of end-binding protein 1 activity by glutathionylation. *Sci. China Life Sci.* **64**, 575–583
48. Ran, J., Liu, M., Feng, J., Li, H., Ma, H., Song, T., Cao, Y., Zhou, P., Wu, Y., Yang, Y., Yang, Y., Yu, F., Guo, H., Zhang, L., Xie, S., *et al.* (2020) ASK1-mediated phosphorylation blocks HDAC6 ubiquitination and degradation to drive the disassembly of photoreceptor connecting cilia. *Dev. Cell* **53**, 287–299.e285
49. Zhang, Y., Lu, J., and Liu, X. (2018) MARCH2 is upregulated in HIV-1 infection and inhibits HIV-1 production through envelope protein translocation or degradation. *Virology* **518**, 293–300
50. Duan, L. W., Zhang, H., Zhao, M. T., Sun, J. X., Chen, W. L., Lin, J. P., and Liu, X. Q. (2017) A non-canonical binding interface in the crystal structure of HIV-1 gp120 core in complex with CD4. *Sci. Rep.* **7**, 46733
51. Odenwald, M. A., Choi, W., Buckley, A., Shashikanth, N., Joseph, N. E., Wang, Y., Warren, M. H., Buschmann, M. M., Pavlyuk, R., Hildebrand, J., Margolis, B., Fanning, A. S., and Turner, J. R. (2017) ZO-1 interactions with F-actin and occludin direct epithelial polarization and single lumen specification in 3D culture. *J. Cell Sci.* **130**, 243–259
52. Perez-Riverol, Y., Csordas, A., Bai, J., Bernal-Llinares, M., Hewapathirana, S., Kundu, D. J., Inuganti, A., Griss, J., Mayer, G., Eisenacher, M., Pérez, E., Uszkoreit, J., Pfeuffer, J., Sachsenberg, T., Yılmaz, Ş., *et al.* (2019) The PRIDE database and related tools and resources in 2019: Improving support for quantification data. *Nucleic Acids Res.* **47**, D442–D450